Engineering Solid Mechanics 6 (2018) 371-389

Contents lists available at GrowingScience

Engineering Solid Mechanics

homepage: www.GrowingScience.com/esm

Progressive damage response and crack growth direction for multiple through cracks of laminated composite finite plate

Pawan Kumar Arora[a*], Sharad Chandra Srivastava[b], M.K.Lohumi[a] and Harish Kumar[c]

[a]*Galgotias College of Engineering & Technology, Greater Noida, India*
[b]*Birla Institute of Technology, Mesra , Ranchi, Jharkhand*
[c]*National Institute of Technology, New Delhi, India*

ARTICLEINFO

Article history:
Received 10 June, 2018
Accepted 5 September 2018
Available online
5 September 2018

Keywords:
Progressive stress intensity factor
Failure load
Subroutine and extended finite element method

ABSTRACT

The present work predicts the numerical progressive failure response and crack growth of finite plate laminated composites with cutout and multiple cracks under in-plane tensile and compressive loads. The ply to ply failure response of the finite plate is predicted using ABAQUS user define field variables subroutine approach, whereas the extended finite element method is used for examination of crack growth direction for multiple through crack of laminated composite finite plate. The subroutine predicted results are compared and validated with published experimental results and extended finite element method results. The effect of changing mesh size, fibre orientation, crack length, crack inclination angle on failure load, progressive stress intensity factor and damage toughness of various crack types is presented and discussed.

© 2018 Growing Science Ltd. All rights reserved.

1. Introduction

The failure or damage of composites is generally preceded by progressive damage response of structure. The evaluation of complex failure mechanisms of laminated composites is big challenge and practical importance in design. Firstly, fracture of composites is a type of fiber breakage, matrix damage and fiber/matrix interface debonding which reduces stiffness and strength (Reddy et al., 1995; Lee & Šimunović 2006; Spottswood & Palazotto 2001; Hühne, 2010). Secondly, delamination may occur due to reduced bonding strength between surrounding layers which mainly depends on polymer matrix (Ogihara & Takeda, 1995; Maimi et al,, 2011; Chen et al, 2004; Hallett et al. 2008).

Stress analysis of various types of cracks is carried out by solving the equations for stress intensity factors (SIFs) under mixed tensile-shear loads (Ameri et al. 2011; Aliha and Saghafi 2013; Ayatollahi and Aliha 2011; Bahmani et al. 2017; Aliha et al. 2015; Ayatollahi et al. 2011). A new numerical model (Srivastava and Lal, 2013; Srivastava et al., 2018: Arora et al., 2017) for calculation of geometrical factor for multiple cracks is developed for aluminium alloy. Many papers (Xie & Biggers, 2006; Sun et al., 2011; Liu et al., 2011; Papanikos, 2005; De Morais & De Moura, 2005) have been published in literatures during past decades on failure models, using numerical or experimental methods for progressive failure analysis of composites.

* Corresponding author.
E-mail addresses: pawanar@rediffmail.com (P. K. Arora)

© 2018 Growing Science Ltd. All rights reserved.
doi: 10.5267/j.esm.2018.9.003

In finite element (FE) approach, if analysis is to be performed on various types of cracks sizes, geometry and their locations than it is necessary to apply remeshing of crack domain whereas in XFEM geometric dimension of crack is independent of FE meshing (Wang et al., 2011). Modeling of moving discontinuities with conventional finite element method is cumbersome due to need to update mesh to match geometry of discontinuity. Discontinuous enrichment functions are used in the extended finite element approximation to account for presence of crack (Belytschko & Black, 2016; Moes et al. 1999). The main advantage is ability of method taking into consideration a crack without any explicit meshing of crack surfaces, and growth of crack can readily be applied without any re-meshing (Asadpoure et al. 2006; Giner et al., 2009; Moes et al., 1999). The XFEM approach (Srivastava & Lal, 2013) is used for prediction of failure loads, fracture toughness for multiple-edge cracks of aircraft material (aluminium alloy). Experiments are performed on different edge crack configurations and are validated with XFEM results.

The proposed numerical approach will be helpful while analyzing the damage tolerance behavior of structure. The present work also examines the parameters affecting the failure response and crack growth direction for laminated composites having cutout and multiple cracks.

2. Specimen details

The fracture parameters of finite plate having cutout and multiple cracks are studied under compressive and tensile loading. The details of specimen along with material orientation axes are

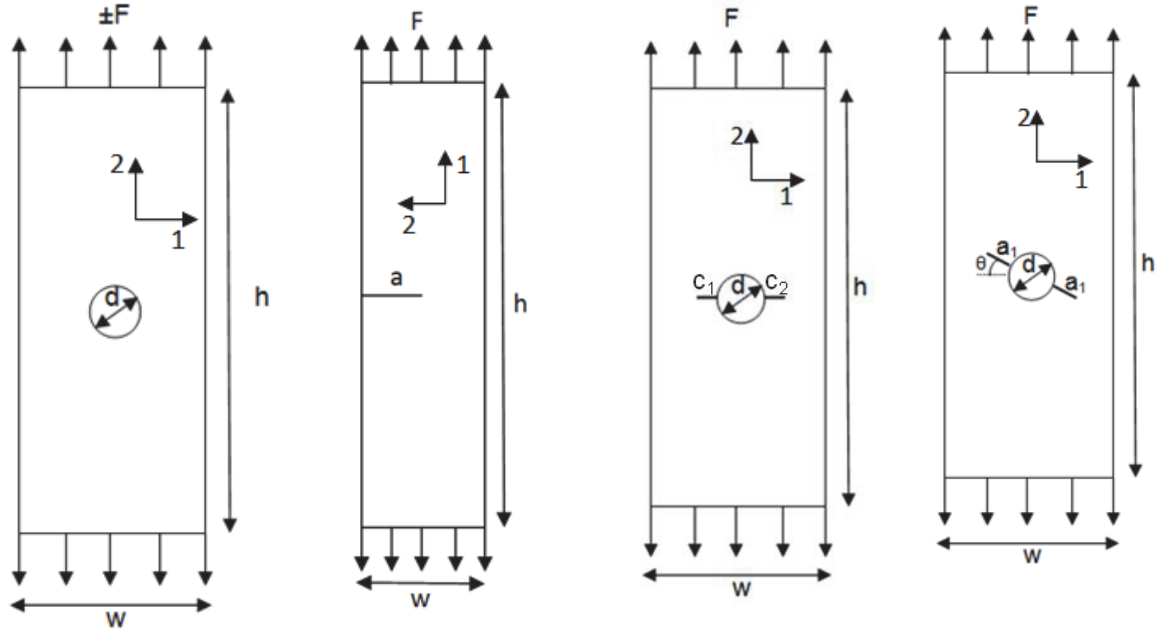

(a) (b) (c) (d)

Fig.1. Details of specimen (a) finite plate with circular cut-out, (b) finite plate with edge crack (c) finite plate with multiple through crack and cutout, (d) finite plate with multiple slanted edge crack and cutout shown in Figs.1 (a-d)

The details of mechanical properties of laminated composite and the specimen details is presented in Table 1-2 respectively.

Table 1. Mechanical properties

Material	t mm	E_1 MPa	E_2 MPa	V	G_{12} MPa	X_T MPa	X_C MPa	Y_T MPa	Y_C MPa	S MPa	Fracture Energy, (N/mm)	
											t_{nf}	t_{sf}
Graphite epoxy	0.14	156512	12962	0.23	6964	-	2707	102.4	253	106.9	-	-
Carbon fiber/epoxy resin	0.3	119100	10760	0.511	6514	-	-	-	-	-	-	-
Carbon fiber epoxy resin	0.13	146800	11400	0.3	6100	1730	1379	66.5	268	58	1	1.5

Table 2. Specimen details

Details of specimen	Configurations, mm	Material
Finite plate with cutout , Fig. 1(a)	w = h/4, d = 6.4, tp = 0.14, t =3.4	Graphite epoxy
	w = h/8, d = 6.4, t_p = 0.13, t = 2.6	Carbon fiber epoxy resin
	w = h/4, d = 6, tp = 0.14, t = 3.4	Carbon fiber epoxy resin
Finite plate with edge crack, Fig.1(b)	w = h/11, a = w/2, tp = 0.3 ,t = 1.2	Carbon fiber/epoxy resin
Finite plate with cutout , and multiple through crack, Fig.1(c)	w = h/4, d = 6, c_1 = c_2 = 1,3, and 5, t_p = 0.14, t = 3.4	Carbon fiber epoxy resin
Finite plate with cutout , with multiple slanted edge crack, Fig. 1(d)	w =h/4, d=6, a_1 = 3, θ = 45^0, t_p = 0.14, t = 3.4	Carbon fiber epoxy resin

3. Methodology

The present research focuses on estimation of failure load, progressive SIF and fracture toughness of laminated composite plate using FE software (ABAQUS) considering compressive and tensile load conditions. The ABAQUS software has been preferred over other software packages as it can be easily customized for subroutines using USDFLD. The subroutine technique incorporates the feasibility in simulation of failure behavior of composite parts which is directly unavailable in the software. Few typical results of subroutine method are validated with published experimental and XFEM results and shows an excellent agreement.

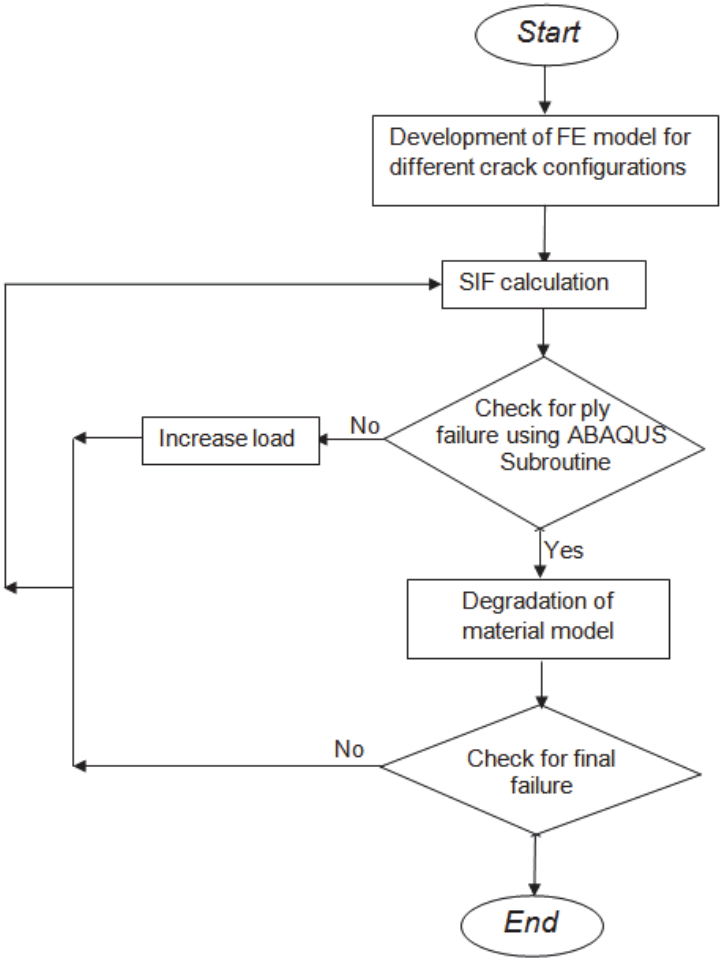

(a)

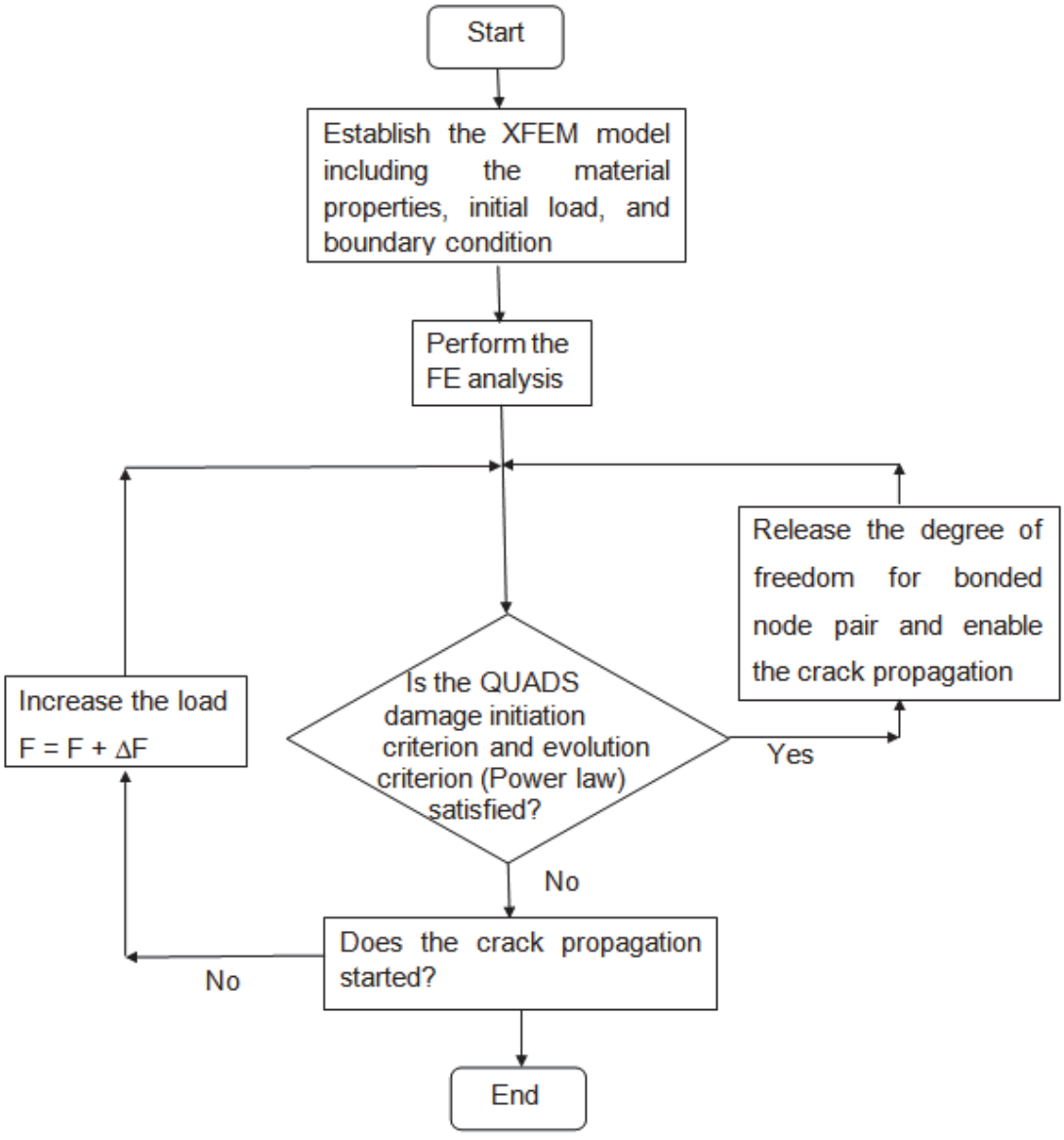

(b)

Fig. 2. Flow chart of the progressive damage using (a) subroutine approach, and (b) XFEM approach

The XFEM results of ply to ply damage load is based on quads damage initiation and power law evolution criteria, discussed in subsequent section 3.1 to 3.2 whereas, Chang and Hashin failure criterion are used for estimation of fracture parameters using subroutine option as discussed in section 4. The subroutine method is used to evaluate the load in elastic as well as progressive failure zone and SIF using J-integral (Rice, 1968). The systematic overview for prediction of failure load, and SIFs using subroutine and XFEM approach are presented in Fig.2 (a-b).

3.1. Damage Initiation

Damage initiation is referred as commencement of degradation of a material (Li & Chandra, 2003; Camanho & Davila, 2002; Abaqus analysis user's manual, 2012). Degradation of a material initiates when the fracture parameters satisfy certain failure initiation criterions. Fig. 3 shows a typical traction-

separation response with a failure mechanism. A value of 1 or higher indicates that initiation criterion has been satisfied. Several damage initiation criteria are available and are discussed below.

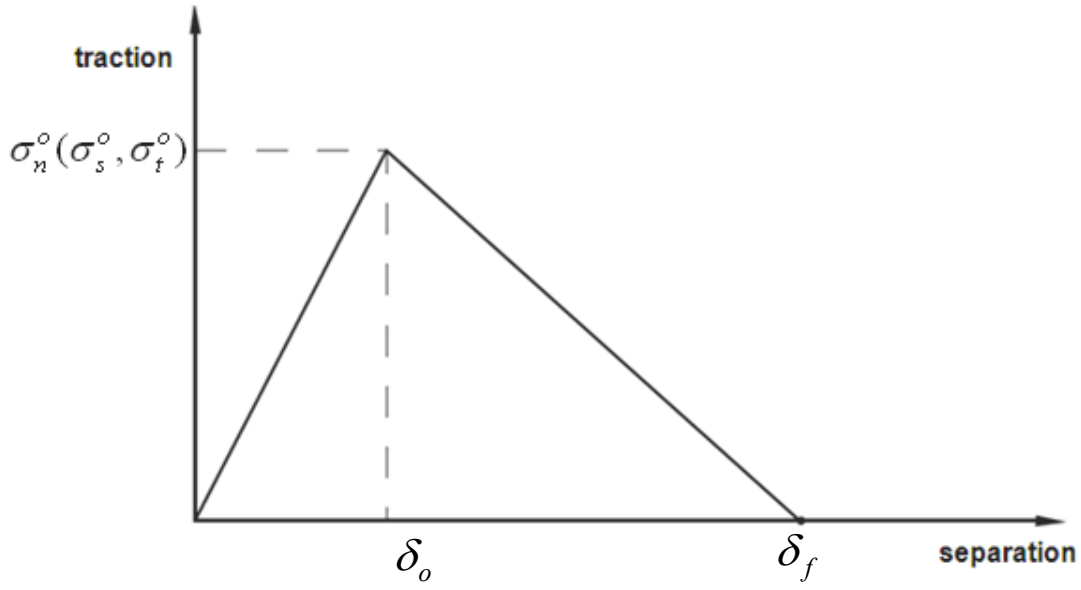

Fig. 3. Typical traction-separation response

3.1.1. QUADS Failure Criterion

In QUADS failure criterion, when the maximum normal stress ratio attains a value equal to one , the failure said to have initiated and is expressed as

$$\max\left\{\frac{\sigma_n}{\sigma_n^o}, \frac{\sigma_s}{\sigma_s^o}, \frac{\sigma_t}{\sigma_t^o}\right\} = 1 \tag{1}$$

3.2. Damage Evolution

The damage evolution explains the rate at which specimen stiffness is downgraded. D, represents overall damage variable in material and defines the combined effects of all the active mechanisms. The initial value of D is zero and in damage evolution its value changes from 0 to 1. The stress components of traction-separation model are affected by damage and can be expressed as:

$$\begin{aligned} \sigma_{nd} &= (1-D)\bar{\sigma}_n \\ \sigma_{sd} &= (1-D)\bar{\sigma}_s \\ \sigma_{td} &= (1-D)\bar{\sigma}_s \end{aligned} \tag{2}$$

Power law fracture criterion defines the interdependency between fracture energy and mode mix. It states that fracture under mixed-mode conditions is ruled by a power law interaction of energies required to cause failure in individual (normal and two shear) modes. It is expressed as

$$\left\{\frac{G_n}{G_n^c}\right\}^\beta + \left\{\frac{G_s}{G_s^c}\right\}^\beta + \left\{\frac{G_t}{G_t^c}\right\}^\beta = 1 \tag{3}$$

4. Degradation of material models

Once damage is predicted by failure criteria, material propoties of composites decreases as per mode of damage, type of dicsontinuties, and nature of loading. Many different degradation models have been proposed during last years (Papanikos et al., 2005; Benabou et al., 2002). In general, degradation material models can be classified in following three groups as shown in Fig.4.

i. Instantaneous degradation : material propoerties are degraded instantaneously to zero, that fit very well as behaviour of brittle materials.

ii. Gradual unloading: material properties are gradually degraded until zero according to a particular unloading curve.

iii. Constant stress: material properties are degraded in order to keep constant the local stress.

For accurate simulation of damage growth, the failure analysis should be capable of predicting the type of failure mode in each ply. Further the stiffness of ply is get reduced and applied correspondingly. Table 3 shows material properties for modes of failure for field variables namely FV_M, FV_F, and FV_S. The FE predictions are based on these three field variables. FV_M, FV_F, and FV_S represents matrix, fiber and shear failure respectively. The undamaged state of composite failure has been assigned as zero value. As the value of any field variable is greater than equal to one, the corresponding damage initiates and degradation of composite starts as per the degradation rule.

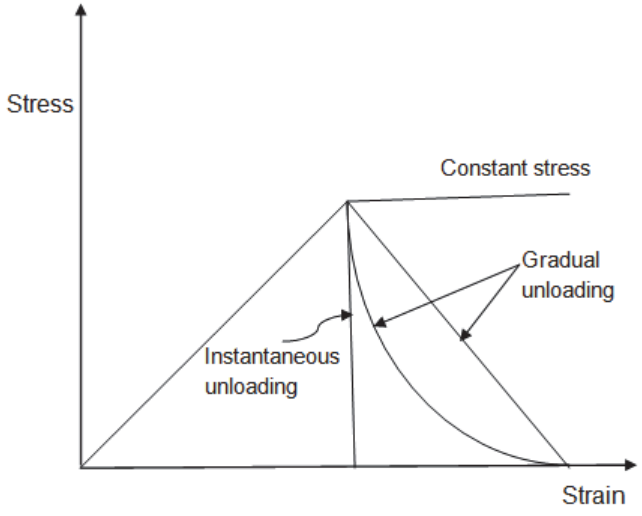

Fig. 4. Post failure degradation curve

In present work Hashin and Chang (Rotem, 2004; Chang & Lessard, 1991) failure criteria are used for prediction of composite modes of failure. The field variables are calculated by Hashin and Chang failure criteria and degradation of stiffness is evaluated by Eq. (4).

$$\begin{aligned} E_1^d &= (1-\alpha)E_1 \\ E_2^d &= (1-\alpha)E_2 \\ G_{12}^d &= (1-\alpha)G_{12} \end{aligned} \tag{4}$$

The failure analysis cannot consider the 100% degradation of composites due to illness of solution. Therefore, the degraded stiffness value is taken as the stiffness corresponding to the failure index of one for each mode of damage i.e. fiber, matrix or shear.

Table 3. Dependence of elastic material properties on Fv's

S. No.	Failure	E_1	E_2	v	G_{12}	FV_M	FV_F	FV_S
1	No failure	E_1	E_2	v	G_{12}	0	0	0
2	Matrix failure	E_1	E_2^d	0	G_{12}	1	0	0
3	Fiber failure	E_1^d	E_2	0	G_{12}^d	0	1	0
4	Matrix-fiber	E_1	E_2^d	0	G_{12}^d	1	1	0
5	Shear failure	E_1	E_2	v	G_{12}^d	0	0	1
6	All failure	E_1	E_2^d	0	G_{12}^d	1	1	1

4.1. Hashin Damage Mechanism

Hashin (Rotem, 2004) had proposed four types of mechanisms of damage initiation namely tensile and compressive fiber failure and tensile and compressive matrix failure as discussed below
Tensile fiber failure index $(\sigma_{11} \geq 0)$ can be written as

$$FV_F^2 = \left(\frac{\sigma_{11}}{X_T}\right)^2 + \left(\frac{\sigma_{12}}{S}\right)^2. \tag{5}$$

Compressive fiber failure index $(\sigma_{11} < 0)$ can be written as

$$FV_F^2 = \left(\frac{\sigma_{11}}{X_C}\right)^2. \tag{6}$$

Tensile matrix failure index ($\sigma_{22} \geq 0$) can be written as

$$FV_M^2 = \left(\frac{\sigma_{22}}{Y_T}\right)^2 + \left(\frac{\sigma_{12}}{S}\right)^2. \tag{7}$$

Compressive matrix failure index $(\sigma_{22} < 0)$ can be written as:

$$FV_M^2 = \left(\frac{\sigma_{22}}{Y_c}\right)^2 + \left(\frac{\sigma_{12}}{S}\right)^2. \tag{8}$$

4.2. Chang Damage Mechanism

As the damage initiates, the material stiffness gets degraded. Chang and Lessard (1991) had proposed the basic modes of fracture of laminated composite structure. These failure modes are: matrix cracking, fiber-matrix shear fracture and fiber fracture.

4.2.1. Matrix Cracking Failure

The failure behavior must satisfy the following condition for nonlinear shear behavior under tensile loading.

$$FV_M^2 = \left(\frac{\sigma_{22}}{Y_T}\right)^2 + \frac{2\sigma_{12}^2 / G_{12} + 3\eta\sigma_{12}^4}{2S^2 / G_{12} + 3\eta S^4}. \tag{9}$$

4.2.2. Fiber Breakage Failure

The failure behaviour must satisfy the following condition for fiber breakage failure under tensile loading.

$$FV_F^2 = \left(\frac{\sigma_{11}}{X_C}\right)^2 + \frac{2\sigma_{12}^2 / G_{12} + 3\eta\sigma_{12}^4}{2S^2 / G_{12} + 3\eta S^4}. \tag{10}$$

4.2.3. Shear Failure

The failure behavior must satisfy the following condition for shear failure of laminated composites.

$$\gamma_{12} = \frac{\sigma_{12}}{G_{12}} + \eta\sigma_{12}^3. \tag{11}$$

Further the Eq. (11) can be expressed as

$$\sigma_{12}^{i+1} = \frac{G_{12}}{1 + \eta G_{12}\left(\sigma_{12}^i\right)^2}\gamma_{12}^{(i+1)}. \tag{12}$$

Eq. (12) is further optimized by using stability analysis and given as

$$\sigma_{12}^{i+1} = \frac{1 + \left(2\eta\left(\sigma_{12}^i\right)^3\right)/\gamma_{12}^i}{1 + 3\eta G_{12}\left(\sigma_{12}^i\right)^2} G_{12}\gamma_{12}^{(i+1)}. \tag{13}$$

For shear damage parameters of ds, Eq. (13) is further reduced to

$$\sigma_{12}^{i+1} = \left(1 - FVs\right)G_{12}\gamma_{12}^{(i+1)}, \tag{14}$$

where,

$$FVs = \frac{3\alpha G_{12}\left(\sigma_{12}^i\right)^2 - 2\alpha\left(\sigma_{12}^i\right)^3/\gamma_{12}^i}{1 + 3\eta G_{12}\left(\sigma_{12}^i\right)^2}. \tag{15}$$

5. Finite element formulation

Fig. 5(a) shows typical XFEM mesh for finite plate with cutout. Specimen is divided in three region i.e. region - 1, 2 and 3. Region - 1 and 3 are for loading and application of boundary conditions whereas; region-2 is for crack growth simulation. Refined mesh in around crack tip is generated to capture the rapidly varying crack growth with respect to time. The fracture parameters are approximated by 8-noded linear hex element (C3D8R). Tensile loading on top edge of region-1 is applied gradually and finite element model is constrained on bottom edge of region-3. The XFEM predicted results are compared with published experimental results.

The XFEM is extended form of traditional finite element approach. It provides the provision for addition of degree of freedom in elements. The mesh size and the actual geometrical size of crack may vary in dimension and the end result remains unaffected. The XFEM approach is useful in simulating the initiation and propagation of a typical crack without remeshing.

In XFEM approach, the following approximation is used to evaluate the displacement of point x locating within the domain (Lin et al., 2012)

$$u^h(x) = u^{FE} + u^{enrichement} \tag{16}$$

$$= N_j(x)\left[\sum_{j=1}^{n} u_j + \sum_{k=1}^{m} \psi(x) a_k\right], \tag{17}$$

where u_j is the vector of regular degrees of nodal freedom in FEM, a_k is the added set of degrees of freedom to the standard FE model and ψ (x) is the discontinuous enrichment function. In Eq. (17), the first term is for approximation the displacement and second term for enriched approximation which accommodates the discontinuities in FE method.

Moes et al. (1999) rearranged the Eq. (17) in order to model crack surface and tip in XFEM method as follows:

$$u^h(x) = \sum_{j=1}^{n} N_j(x) u_j + \sum_{h=1}^{m} N_j(x)\left(H(\xi(x))a_h + \sum_{k=1}^{mt_1} N_j(x)\left(\sum_{l=1}^{mf} (F_l^1(x) b_k^{l1}\right)\right.$$

$$\left. + \sum_{k=1}^{mt_2} N_j(x)\left(\sum_{l=1}^{mf} (F_l^2(x) b_k^{l2}\right)\right). \tag{18}$$

where,

m is the set of nodes having crack face

mt_1 and mt_2 are the sets of nodes for crack tips 1 and 2

a_h is the enriched nodal DOF vector associated with Heaviside enrichment function

b_k^{l1} and b_k^{l2} is the enriched nodal DOF vector associated with the asymptotic crack-tip functions

u_j are the nodal displacements associated with the continuous part of the finite element solution

N_j is finite element shape functions

F_l^1 & F_l^2 represent the mf crack tip enrichment functions.

In Eq. (18), the first term is for approximation of displacement and second term is for XFEM expression of displacement at crack face whereas third and fourth terms is representing the displacement field at crack tip 1, and 2 respectively.

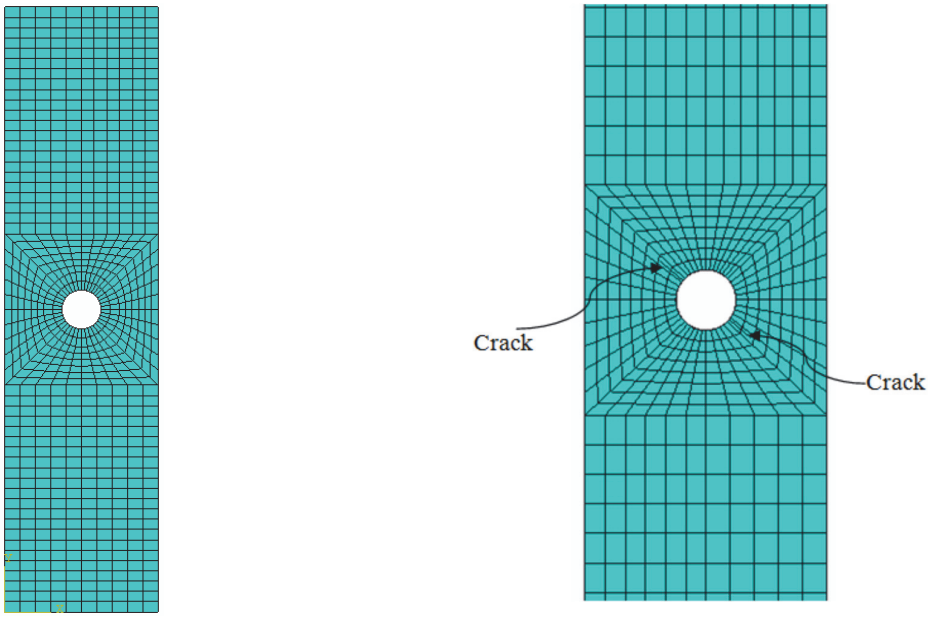

(a) (b)

Fig. 5. Typical meshed model for (a) XFEM, and (b) USDFLD

Fig. 5(b) shows a USDFLD mesh for a composite plate with cutout. Refined meshed is used around discontinuity. Eight-noded iso-parametric quadratic element (S8R5) is used in present work. The FE model is constrained at bottom edge, whereas entire load is uniformly distributed over nodes of top edge.

6. Results and discussion

The validation of predicted results of present work is compared with various published experimental results for different configurations and discussed as under.

Table 4. Validation of compressive failure load with published experimental work

Specimen details, mm Refer Fig. 1(a)	Lay-up	Published Experimental work , Ref. ((Chang and Lessard, 1991)	Present work, USDFLD		
		Load (N)	c	α (%)	Load (N)
w = h/4, d = 6.4,			d/4		13519
t_p = 0.14,	[(±45)$_{12}$]s	13500	d/5	85	13092
t = 3.4			d/6		13230

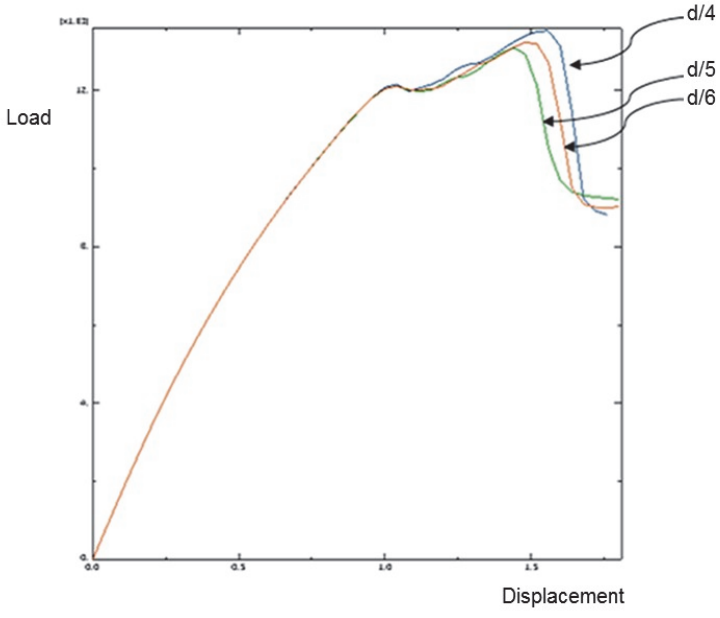

Fig. 6. Force versus displacement curve of different mesh size

6.1. Validation of Compressive Failure Load using Subroutine

Table 4 shows validation of subroutine predicted compressive failure load with published experimental work (Chang & Lessard, 1999) of a finite plate with cut-out .The failure load is estimated considering different mesh size as d/4, d/5, and d/6. The plate is made of 24 plies of graphite-epoxy for a lay-up $[(-45/+45)_6]_S$. Each ply has a thickness of 0.14 mm, and total thickness of plate is 3.4 mm. FE predicted failure load shows an excellent agreement with respect to published work for mesh size of d/4. The best agreement of failure load is seen for degradation factor of 85%. Fig. 6 shows subroutine prediction of load versus displacement curve, shows damage on specimen starts at load of 12,270 N whereas, maximum load carrying capacity of specimen is 13,500 N. Fig. 7(a-c) show predefined FVs plot for fiber, matrix and shear damage. First, damage starts with matrix failure as weft strength and stiffness are less and afterward damage starts on fiber.

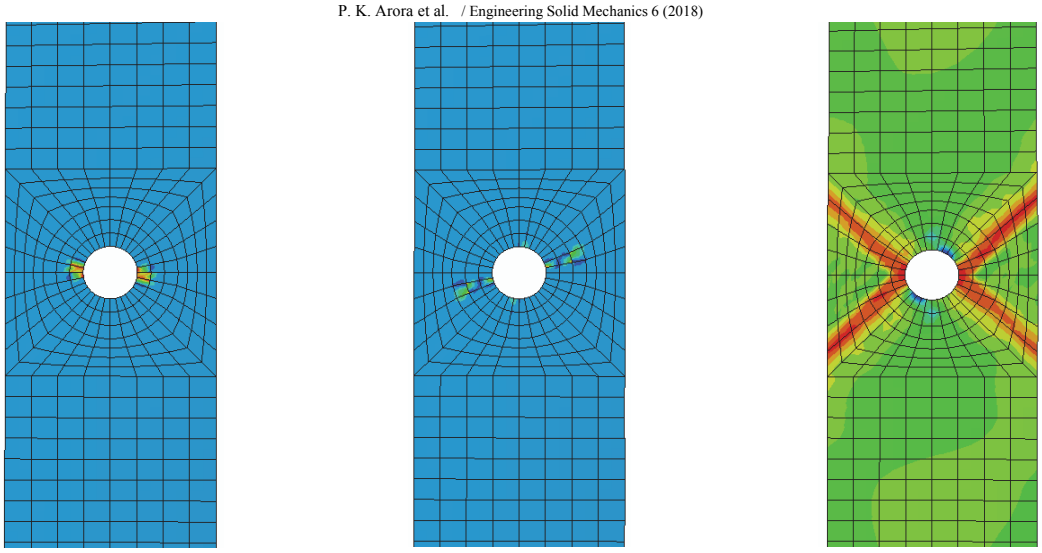

(a) (b) (c)

Fig. 7. Predefined field variable for (a) matrix failure, (b) fiber failure, and (c) shear damage

6.2. Validation of Tensile Failure Load using XFEM and User Defined Field Variables

Table 5(a) shows the validation of XFEM predicted failure load of a finite plate with cut-out under tensile loading with published experimental work (Tan, 1991). The individual ply thickness is 0.13 mm and total thickness is 2.6 mm. The XFEM prediction of failure load is considered for two lay-up such as $[0/(\pm45)_3/(90)_3]s$, and $[0/(\pm45)_2/(90)_5]s$ and shows an excellent agreement with published experimental work for mesh size of d/4. In both lay-ups first damage starts for plies in direction of 90^0, and afterward damage propagates to 45^0 and 0^0 of plies. Plies with 90^0 orientations are weakest lamina as transverse stiffness and weft strength is lowest. Once, crack is initiated and propagated through cut-out for 90^0 plies, load bearing capacity decreases gradually which shows gradual degradation of material properties.

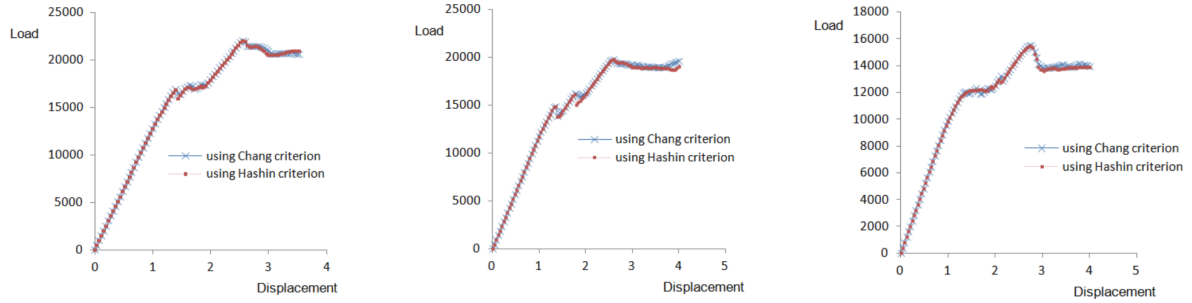

(a) (b) (c)

Fig. 8. Force versus displacement curve for (a) lay-up $[0/(\pm45)_3/(90)_3]s$,(b) $[0/(\pm45)_2/(90)_5]s$, and (c) $[0/(\pm45)/(90)_7]s$

Table 5a. Validation of XFEM predicted tensile failure load with published experimental work

Specimen details, mm Refer Fig. 1(a)	Lay-up	Failure load(N)			
		Published Experimental work, Ref.(Lin et al., 2012)	Present work XFEM		
			c	Without crack	with crack $a_1 = a_2 = 3$ mm, $\theta = 40^0$
w = h/8, d = 6.4, t_p = 0.13 t = 2.6	$[0/(\pm45)_3/(90)_3]s$	23580	d/4.3	26504 (12.4%)	-
			d/4.5	25402 (7.7%)	11270
	$[0/(\pm45)_2/(90)_5]s$	18580	d/4.5	18863 (1.5%)	6049

Table 5b. Validation of subroutine predicted failure load with published experimental work

Specimen details, mm Refer Fig. 1(a)	Lay-up	Failure load(N)			
		Published Experimental work , Ref(Lin et al., 2012)	Present work Subroutine		
			c	Using Chang criterion	Using Hashin criterion
w = h/8, d = 6.4, t_p = 0.13, t = 2.6	$[0/(\pm45)_3/(90)_3]s$	23580	d/4	22032 (-6.6%)	22057 (-6.5%)
	$[0/(\pm45)_2/(90)_5]s$	18580		19774 (6.4%)	19801 (6.6%)
	$[0/(\pm45)/(90)_7]s$	16000		15524 (2.9%)	15435 (3.5%)

Table 5(b) shows the validation of subroutine predicted failure load using Chang and Hashin failure criterion with published experimental work (Tan, 1991). The subroutine prediction of failure load is considered for three lay-up $[0/(\pm45)_3/(90)_3]s$, $[0/(\pm45)_2/(90)_5]s$, and $[0/(\pm45)/(90)_7]s$. Predicted failure load shows an excellent agreement with published experimental work with a mesh size of d/4. Fig. 8 (a-c) show load versus displacement curve. Predicted load using Chang criterion show an excellent agreement with Hashin predicted load. The subroutine predicted load for three lay-up show an excellent agreement with published experimental work. Maximum variation between Chang and Hashin predicted failure results with respect to experimental load is -6.6%, and -6.5% respectively.

6.3. Effect of Ply Orientation on Failure Load and Crack Growth Direction

Fig. 9 shows variation of load with respect to displacement of a finite composite plate with cut-out for lay-up $[(\pm60)_{12}]_s$, and $[(\pm90)_{12}]_s$ using XFEM. The XFEM predicted failure strength for lay-up $[(\pm90)_{12}]_s$ is less than $[(\pm60)_{12}]_s$, as transverse stiffness and strength for $\pm90^0$ fiber orientation is lower than effective stiffness and strength of fiber orientation $\pm60^0$, shown in Table 6 . Figs. 10 (a-b) show the XFEM predicted crack initiation and growth for lay-up $[(\pm60)_{12}]s$, and $[(\pm90)_{12}]s$. Crack initiation and propagation for both case is observed in transverse fiber direction as strength and stiffness of specimen is less. Crack is initiated from hole due to stress concentration and propagated in four directions for lay-up $[(\pm60)_{12}]s$ whereas, crack is initiated and propagated perpendicular to loading for lay-up $[(\pm90)_{12}]s$ as transverse strength and stiffness is less.

Table 6. Effect of ply orientation on failure load

Specimen details, mm Refer Fig. 1(a)	Lay-up	Failure load, N XFEM
w = h/4, d = 6,	$[(\pm60)_{12}]s$	4463
t_P = 0.14, t = 3.4	$[(\pm90)_{12}]s$	3912

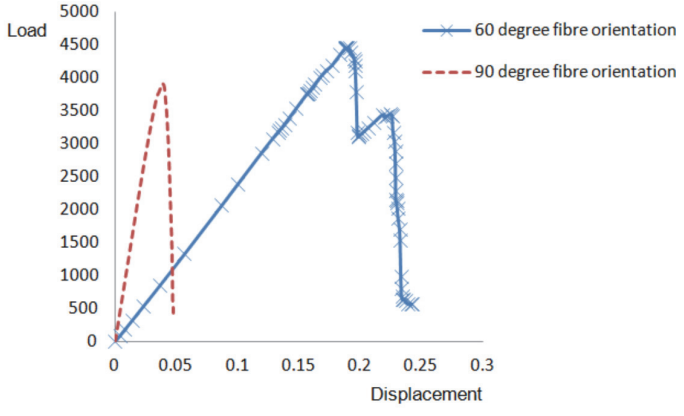

Fig. 9. Force versus displacement curve for lay-up $[(\pm60)_{12}]s$, and $[(\pm90)_{12}]s$

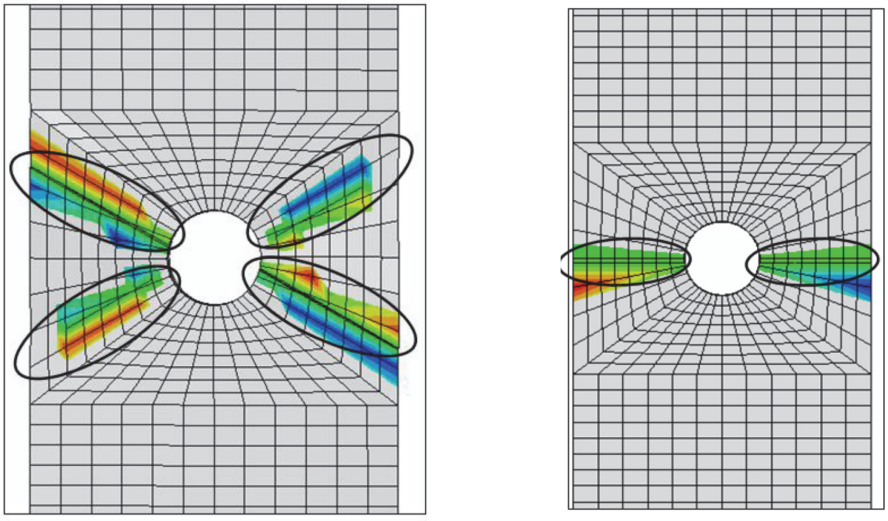

(a) (b)

Fig. 10. Effect of lay-up on crack initiation and growth direction for (a) lay-up $[(\pm 60)_{12}]$s, and (b) lay-up $[(\pm 90)_{12}]$s.

6.4. Examination of SIF for Single Edge Crack

The SIF values of present work are compared with the experimental results of published work (Kaman 2011) for different orientation and are tabulated in Table 7. The SIF values for different orientation are in good agreement with the experimental work. As fiber orientation is increasing from $[0^0/15^0]_s$ to $[0^0/90^0]_s$,corresponding failure loads are decreasing, hence value of SIF decreases.

Table 7. Comparison of published work with present work

Lay-up Refer Fig.1(b)	Experimental Ref Moes et al. (1991)		Present work using ABAQUS
	F_L (N)	SIF	SIF
$[0^0/15^0]_S$	6516.112	4404.62	4220
$[0^0/60^0]_S$	5229.024	2873	3310
$[0^0/75^0]_S$	4193.829	2633	2871
$[0^0/90^0]_S$	3680.767	2416	2625

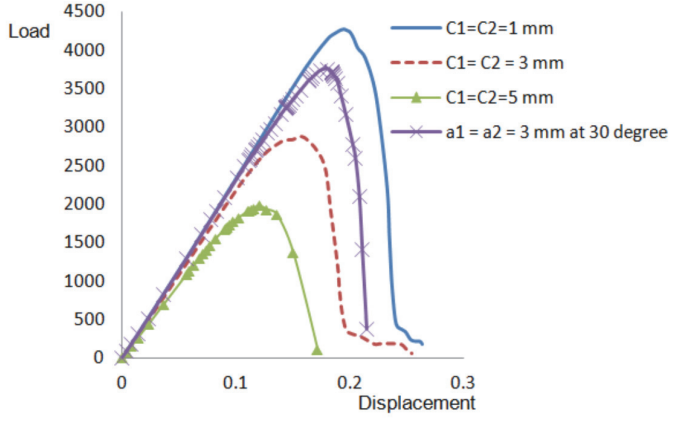

Fig. 11. Force versus displacement curve for different crack configurations for lay-up $[(\pm 60)_{12}]$s using XFEM.

6.5. Effect of Multiple Cracks on Fracture Strength

Fig.11 represents load/displacement curve for lay-up $[(\pm 60)_{12}]s$ with different crack length using XFEM. Figure shows that increase in crack length decreases the load bearing capacity and subsequently reduces the fracture strength.

Table 8 shows comparison of predicted failure load using XFEM and subroutine for multiple crack configurations and shows similar conclusions as in Fig. 11. The subroutine predicted fracture strength with 100% degradation factor shows an excellent agreement with XFEM failure strength for lay-up $[(\pm 60)_{12}]s$. During FE simulation stiffness can-not consider 0 for 100% degradation; hence unit value of stiffness is used for respective stiffness as per mode of damage. Predicted failure loads for different cracks configurations show instantaneous degradation of material properties, which behave as brittle material.

Table 8. Effect of multiple cracks on failure load

Specimen details, mm Refer Figs.1(c-d)	Lay-up with multiple through crack cracks	XFEM	UEDFLD		
		F_L(N)	F_L (N)	F_L (N)	α (%)
			Using Chang Criterion	Using Hashin Criterion	
w = h/4, d = 6, t_p = 0.14, t = 3.4	$[(\pm 60)_{12}]s$ $c_1 = c_2 = 1$	4272	4522	4491	100
	$[(\pm 60)_{12}]s$ $c_1 = c_2 = 3$	2858	2899	2899	
	$[(\pm 60)_{12}]s$ $c_1 = c_2 = 5$	1977	2010	2148	
	$[(\pm 60)_{12}]s$ $a_1 = 3$, $\theta = 30^0$	3762	4065	3991	

Figs.12 (a-e) show crack growth direction for multiple edge cracks configurations for lay-up $[(\pm 60)_{12}]s$, and $[(\pm 90)_{12}]s$ using XFEM. In all cases, cracks are propagating in direction of lower strength and stiffness, which is weft direction. Ply with 90^0 fiber orientation shows more strength than 60^0 fiber as remaining cross-section area for 90^0 fiber orientation in presence of crack is more than fiber with 60^0 fiber orientation as shown in Figs.12 (d -e).

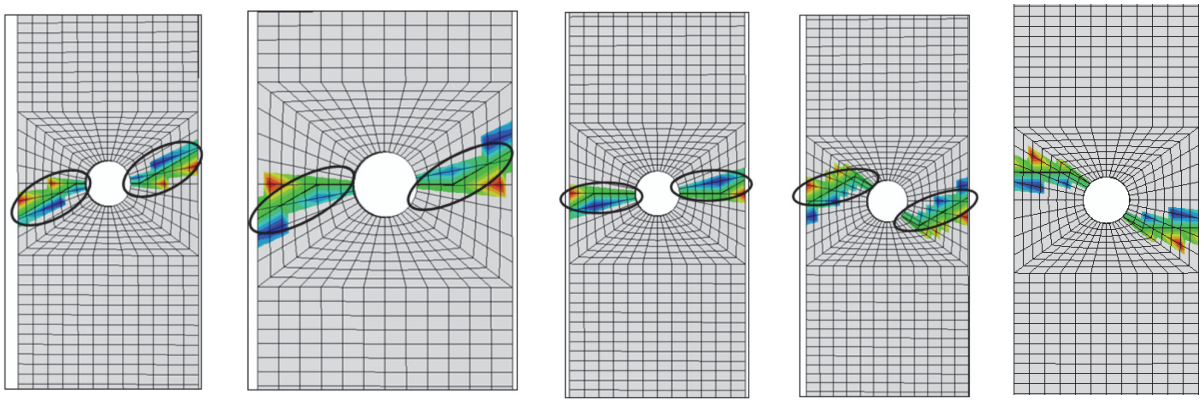

(a) (b) (c) (d) (e)

Fig.12. Crack growth direction for (a) $[(\pm 60)_{12}]s$, $c_1 = c_2 = 1$ mm, (b) $[(\pm 60)_{12}]s$, $c_1 = c_2 = 3$ mm, (c) $[(\pm 60)_{12}]s$, $c_1 = c_2 = 5$ mm, (d) $[(\pm 60)_{12}]s$, $\theta = 30^0$, $a_1 = 3$ mm, and (e) $[(\pm 90)_{12}]s$, $\theta = 45^0$, $a_1 = 3$ mm

6.6. Effect of Degradation on Load

Figs. 13 (a-c) show load versus displacement curve for lay-up [(±45)12]s with a = 1, 3, and 5 mm using Chang criterion and Hashin criterion. In elastic region load is directly proportional to

displacement whereas reverse of it takes place after initiation of damage. Which causes decrease in load with respect to displacement for stiffness degradation model; whereas without stiffness degradation model still suggested that the load is proportional to displacement. Similar trend is seen for crack length of 3 and 5 mm as shown in Figs.13 (b-c). In all multiple crack configurations, predicted load in elastic region using Hashin and Chang criteria show an excellent agreement whereas, maximum percentage difference in predicted load for same value of displacement using these criteria are 5.6% in damage region.

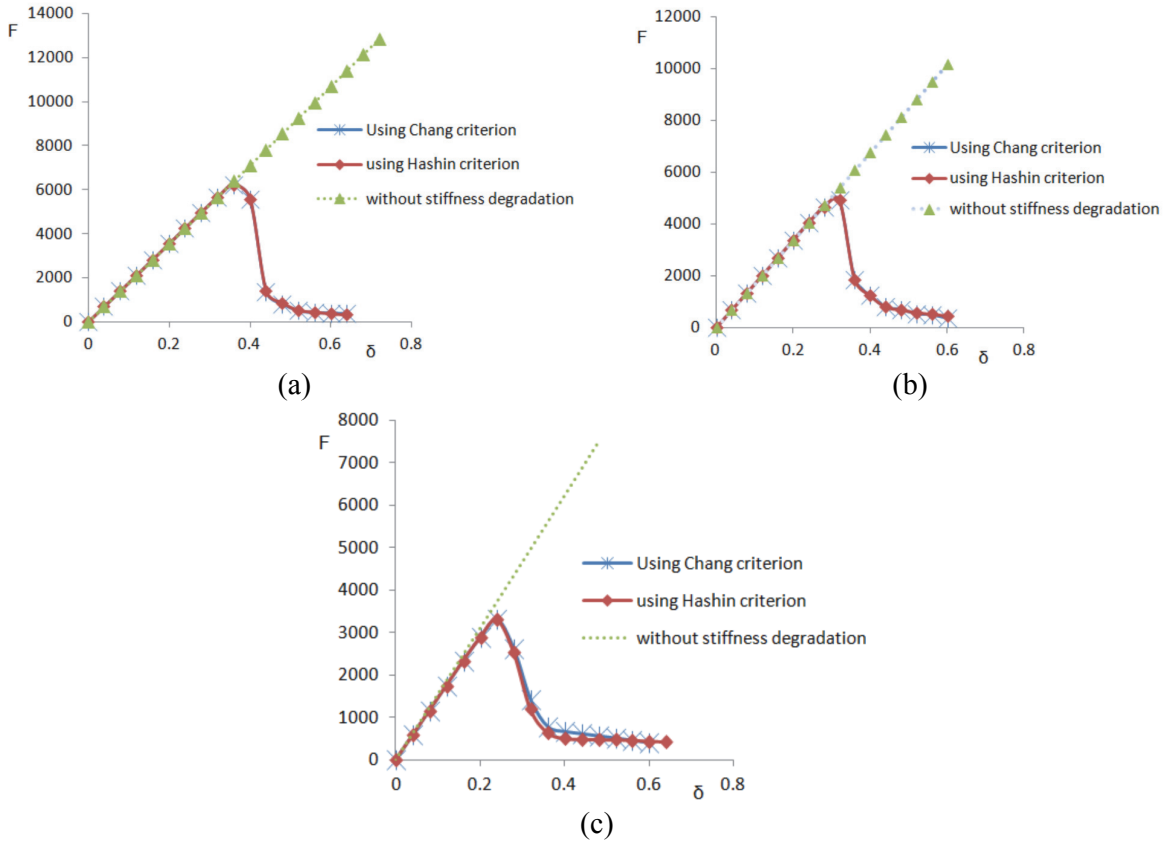

Fig.13. Force versus displacement curve for different crack configurations for lay-up $[(\pm 45)_{12}]s$ (a) crack length = 1 mm, (b) crack length = 3 mm, and (c) crack length = 5 mm

6.7. Effect of Degradation on SIF

Figs.14 (a-c) show load versus mode - I SIF curve for $c_1 = c_2 = 1$, 3, and 5 mm, lay-up $[(\pm 60)_{12}]_S$ respectively with and without stiffness degradation for multiple through crack emanating from cutout. The FE prediction of different crack configurations is considered with twenty four numbers of layers and each layer with thickness of 0.14 mm. Figure 14a shows load versus mode - I SIF curve for $c_1 = c_2 = 1$. As load increases, SIF value increases in elastic region as SIF is directly proportional to load. Once damage starts, SIF with stiffness degradation reduces as load bearing capacity of specimen decreases, whereas SIF without stiffness degradation is still increases. Similar trend is observed for through crack length of 3, and 5 mm as shown in Figs. 14 (b-c). In all multiple crack configurations, FE prediction of SIF, fracture toughness and progressive SIFs using Chang criterion show an excellent agreement with Hashin criterion.

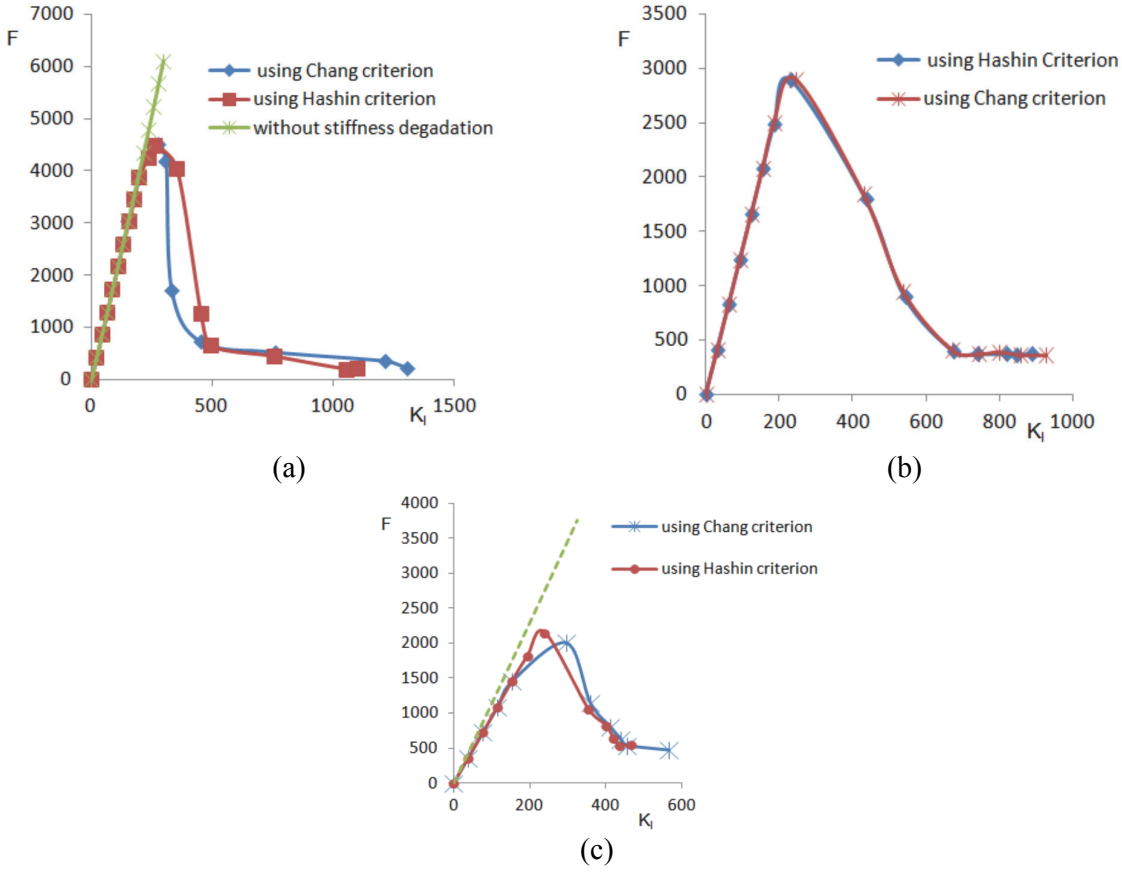

Fig.14. Force versus mode - I SIF for lay-up $[(\pm 60)_{12}]_S$ with and without stiffness degradation, (a) crack length = 1 mm, (b) crack length = 3 mm, and (c) crack length = 5 mm

Table 9 shows fracture toughness versus load value for different cracks configurations and lay-up with and without stiffness degradation using Chang criterion and Hashin criterion. The typical value of fracture toughness of specimen for $c_1 = c_2 = 1$ mm and lay-up $[(\pm 60)_{12}]_s$ are 278, and 261 MPa $(mm)^{1/2}$ corresponding maximum load bearing capacity is 4522, and 4491 N using Chang and Hashin criterion respectively whereas it is 5669 N for same value of SIF with no stiffness degradation . Similar trend is observed for other crack configurations and lay-ups.

Table 9. Fracture toughness versus force

Configuration, mm Refer Figs.1(c-d)	Lay-up	Fracture toughness $MPa(mm)^{1/2}$		Load (N)		
		Using Chang criterion	Using Hashin criterion	Using Chang criterion	Using Hashin criterion	without stiffness degradation
w = h/4, d = 6, $t_p = 0.14$, t = 3.4	$[(\pm 60)_{12}]s$ $c_1 = c_2 = 1$	278	261	4522	4491	5669
	$[(\pm 60)_{12}]s$ $c_1 = c_2 = 3$	245	232	2899	2899	3333
	$[(\pm 60)_{12}]s$ $c_1 = c_2 = 5$	295	240	2010	2148	2914
	$[(\pm 60)_{12}]s$ $a_1 = 3$, $\theta = 30^0$	198	202	4065	3991	4269
	$[(\pm 45)_{12}]s$ $c_1 = c_2 = 1$	415	415	6215	6215	7823
	$[(\pm 45)_{12}]s$ $c_1 = c_2 = 3$	472	473	4922	4922	6760
	$[(\pm 45)_{12}]s$ $c_1 = c_2 = 5$	440	441	3305	3304	4978

6.8. Examination of SIFs for Slanted Through Crack

Figs. 15 (a-b) show load versus SIF curve with and without stiffness degradation for multiple slanted through cracks ($a_1 = 3$ mm, $\theta = 30^0$) with cutout for lay-up $[(\pm 60)_{12}]_S$. Analysis is carried considering twenty four number of layers and each layer with thickness of 0.14 mm. As load increases, SIFs value in mode-I increases in elastic region as SIF is directly proportional to load. Once damage starts, SIF for stiffness degradation reduces as shown in Fig. 15(a). The SIF value with stiffness degradation model suggest that once damage starts, 1889 N load is required for mode-I SIF value of 270 MPa(mm)$^{1/2}$ whereas, without stiffness degradation model suggest 5.6 ton for same value of SIF. Similar trend is seen for mode-II SIF value, shown in Fig. 15(b). The mode - II SIF value increases in elastic zone, and decreases as damage progress.

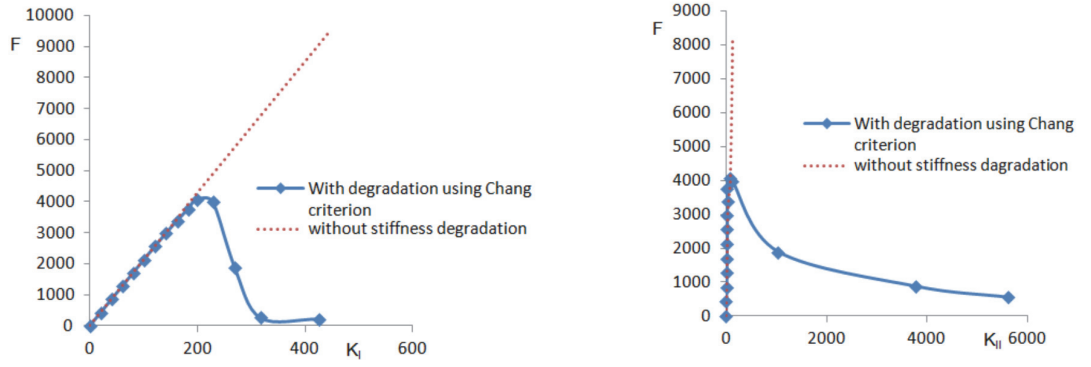

(a) (b)

Fig. 15 Force versus SIF curve for slanted edge crack with material degradation, lay-up $[(\pm 60)_{12}]s$ (a) mode - I SIF, and (b) mode - II SIF

7. Conclusion

Based on analysis results stated above, conclusion is appended as under:

I. Subroutine predicted value of failure load, and SIFs show good agreement with the XFEM and published experimental work.

II. Degradation factor depends on type of discontinuities, fiber orientation and nature of load, and degradation factor.

III. Once damage starts, degradation of laminated composite material decreases gradually for plate with cut-out. Damage of laminated composites is in effective weft direction as stiffness and strength is lower for weft direction.

IV. As crack length increases the failure load decreases as load bearing capacity of specimen reduces. This causes decrease in load with respect to displacement for stiffness degradation model, whereas with no stiffness degradation the load is proportional to displacement.

V. Once damage starts, the SIFs for stiffness degradation decreases as load bearing capacity of specimen reduces. The SIF value of without stiffness degradation still increases. It indicates that in this type of model the fracture parameters are significantly over estimated.

References

Abaqus analysis user's manual, version 6.12, Vol. V (2012). Dassault Systemes Simulia Corp., Providence, RI, USA.

Aliha, M. R. M., & Saghafi, H. (2013). The effects of thickness and Poisson's ratio on 3D mixed-mode fracture. *Engineering Fracture Mechanics*, *98*, 15-28.

Aliha, M. R. M., Bahmani, A., & Akhondi, S. (2015). Numerical analysis of a new mixed mode I/III fracture test specimen. *Engineering Fracture Mechanics*, *134*, 95-110.

Ameri, M., Mansourian, A., Khavas, M. H., Aliha, M. R. M., & Ayatollahi, M. R. (2011). Cracked asphalt pavement under traffic loading–A 3D finite element analysis. *Engineering Fracture Mechanics*, *78*(8), 1817-1826.

Arora, P., Srivastava, S., & Kumar, H. (2017). Determination of crack growth direction for multiple offset edge cracks of a finite plate. *Engineering Solid Mechanics*, *5*(3), 185-198.

Asadpoure, A., Mohammadi, S., & Vafai, A. (2006). Modeling crack in orthotropic media using a coupled finite element and partition of unity methods. *Finite Elements in Analysis and Design*, *42*(13), 1165-1175.

Ayatollahi, M. R., & Aliha, M. R. M. (2011). On the use of an anti-symmetric four-point bend specimen for mode II fracture experiments. *Fatigue & Fracture of Engineering Materials & Structures*, *34*(11), 898-907.

Ayatollahi, M. R., Aliha, M. R. M., & Saghafi, H. (2011). An improved semi-circular bend specimen for investigating mixed mode brittle fracture. *Engineering Fracture Mechanics*, *78*(1), 110-123.

Bahmani, A., Aliha, M. R. M., & Berto, F. (2017). Investigation of fracture toughness for a polycrystalline graphite under combined tensile-tear deformation. *Theoretical and Applied Fracture Mechanics*, *90*, 53-64.

Belytschko, T., & Black, T. (1999). Elastic crack growth in finite elements with minimal remeshing. *International journal for numerical methods in engineering*, *45*(5), 601-620.

Benabou, L., Benseddiq, N., & Naıt-Abdelaziz, M. (2002). Comparative analysis of damage at interfaces of composites. *Composites Part B: Engineering*, *33*(3), 215-224.

Camanho, P. P., & Dávila, C. G. (2002). Mixed-mode decohesion finite elements for the simulation of delamination in composite materials.

Chang, F. K., & Lessard, L. B. (1991). Damage tolerance of laminated composites containing an open hole and subjected to compressive loadings: Part I—Analysis. *Journal of Composite Materials*, *25*(1), 2-43.

Chen, H., Hong, M., & Liu, Y. (2004). Dynamic behavior of delaminated plates considering progressive failure process. *Composite structures*, *66*(1-4), 459-466.

De Morais, A. B., & De Moura, M. F. S. F. (2005). Assessment of initiation criteria used in interlaminar fracture tests of composites. *Engineering fracture mechanics*, *72*(17), 2615-2627.

Giner, E., Sukumar, N., Tarancón, J. E., & Fuenmayor, F. J. (2009). An Abaqus implementation of the extended finite element method. *Engineering fracture mechanics*, *76*(3), 347-368.

Hallett, S. R., Jiang, W. G., Khan, B., & Wisnom, M. R. (2008). Modelling the interaction between matrix cracks and delamination damage in scaled quasi-isotropic specimens. *Composites Science and Technology*, *68*(1), 80-89.

Hühne, C., Zerbst, A. K., Kuhlmann, G., Steenbock, C., & Rolfes, R. (2010). Progressive damage analysis of composite bolted joints with liquid shim layers using constant and continuous degradation models. *Composite Structures*, *92*(2), 189-200.

Kaman, M. O. (2011). Effect of fiber orientation on fracture toughness of laminated composite plates [0°/θ°] s. *Engineering Fracture Mechanics*, *78*(13), 2521-2534.

Lee, H. K., & Šimunović, S. (2006). Prediction of crack evolution and effective elastic behavior of damage-tolerant brittle composites. *Computer Methods in Applied Mechanics and Engineering*, *196*(1-3), 118-133.

Li, H., & Chandra, N. (2003). Analysis of crack growth and crack-tip plasticity in ductile materials using cohesive zone models. *International Journal of Plasticity*, *19*(6), 849-882.

Lin, Z., Zhuang, Z., You, X., Wang, H., & Xu, D. (2012). Enriched goal-oriented error estimation applied to fracture mechanics problems solved by XFEM. *Acta Mechanica Solida Sinica*, *25*(4), 393-403.

Liu, P. F., Hou, S. J., Chu, J. K., Hu, X. Y., Zhou, C. L., Liu, Y. L., ... & Yan, L. (2011). Finite element analysis of postbuckling and delamination of composite laminates using virtual crack closure technique. *Composite Structures*, *93*(6), 1549-1560.

Maimi, P., Camanho, P. P., Mayugo, J. A., & Turon, A. (2011). Matrix cracking and delamination in laminated composites. Part II: Evolution of crack density and delamination. *Mechanics of Materials*, *43*(4), 194-211.

Moës, N., Dolbow, J., & Belytschko, T. (1999). A finite element method for crack growth without remeshing. *International Journal for Numerical Methods in Engineering*, *46*(1), 131-150.

Ogihara, S., & Takeda, N. (1995). Interaction between transverse cracks and delamination during damage progress in CFRP cross-ply laminates. *Composites Science and Technology*, *54*(4), 395-404.

Papanikos, P., Tserpes, K. I., Labeas, G., & Pantelakis, S. (2005). Progressive damage modelling of bonded composite repairs. *Theoretical and Applied Fracture Mechanics*, *43*(2), 189-198.

Reddy, Y. S. N., Moorthy, C. D., & Reddy, J. N. (1995). Non-linear progressive failure analysis of laminated composite plates. *International Journal of Non-Linear Mechanics*, *30*(5), 629-649.

Rice, J. R. (1968). A path independent integral and the approximate analysis of strain concentration by notches and cracks. *Journal of applied mechanics*, *35*(2), 379-386.

Rotem, A. (2004). Prediction of laminate failure with the Rotem failure criterion. In *Failure Criteria in Fibre-Reinforced-Polymer Composites* (pp. 298-315).

Spottswood, S. M., & Palazotto, A. N. (2001). Progressive failure analysis of a composite shell. *Composite Structures*, *53*(1), 117-131.

Srivastava, A. K., & Lal, A. (2014). Dynamic simulation of multiple offset-edge crack of a finite plate. *Journal of Aircraft*, *51*(3), 849-860.

Srivastava, A. K., Arora, P. K., Srivastava, S. C., Kumar, H., & Lohumi, M. K. (2018). Determination of Fracture Parameters for Multiple Cracks of Laminated Composite Finite Plate. *Applied Composite Materials*, *25*(2), 381-398.

Srivastava, A. K., & Lal, A. (2013). Determination of fracture parameters for multiple edge cracks of a finite plate. *Journal of Aircraft*, *50*(3), 901-910.

Sun, X. S., Tan, V. B. C., & Tay, T. E. (2011). Micromechanics-based progressive failure analysis of fibre-reinforced composites with non-iterative element-failure method. *Computers & Structures*, *89*(11-12), 1103-1116.

Tan, S. C. (1991). A progressive failure model for composite laminates containing openings. *Journal of Composite Materials*, *25*(5), 556-577.

Wang, Z., Ma, L., & Wu, L. (2011). Numerical simulation of crack growth through particulate clusters in brittle matrix using the XFEM technique. *Procedia Engineering*, *10*, 786-791.

Xie, D., & Biggers Jr, S. B. (2006). Progressive crack growth analysis using interface element based on the virtual crack closure technique. *Finite Elements in Analysis and Design*, *42*(11), 977-984.

© 2018 by the authors; licensee Growing Science, Canada. This is an open access article distributed under the terms and conditions of the Creative Commons Attribution (CC-BY) license (http://creativecommons.org/licenses/by/4.0/).